



Comprehensive physicochemical study of calcium phosphate nanocrystal ageing process using univariate and bivariate linear regressions

M. Selmi¹, R. Chiriac², S. Somrani^{1*}

¹Université de Tunis, UR15ES01, IPEIT, 2 Rue Jawaher Lel Nahru, 1089 Montfleury, Tunis.

²LMI, Bâtiment Berthollet, 43 Boulevard du 11 novembre 1918, 69622 Villeurbanne Cedex.

Received 29 Jun 2016, Revised 08 Sep 2016, Accepted 20 Sep 2016

*For correspondence: Email: sayda.somrani@yahoo.fr (S. Somrani); Phone: +216 20267726; fax: +216 71337323

Abstract

A series of biomimetic carbonate-free apatites (NHA) was synthesized at physiological pH and different maturation times. We will rely on quantitative correlations, using statistical treatments between labile species, apatitic ones, microstructural parameters and dissolution enthalpy. This study reveals that maturation process follows two phases. The first one starts earlier and is predominated by labile HPO_4^{2-} deprotonation. The second one is slow and associated with the consumption and release of water. It is predominated by two events (i) relocation of labile species to prefigure the apatitic domains (ii) hydrolysis of labile PO_4^{3-} species, into apatitic HPO_4^{2-} and OH^- groups. For the first time, the labile and not the apatitic PO_4^{3-} entities are quantitatively confirmed to be the main cause of aged nanocrystals hydroxylation which happens only if some order established beforehand. So, there's a lack of OH^- in nascent nanocrystals. These findings will clarify the role of each non-apatitic species in bio mineralization process. The young bioapatites reactivity can be controlled by labile HPO_4^{2-} . Then, NHA's senescence is overpowered by bioapatites hydroxylation using labile PO_4^{3-} . Moreover, we can expect early mineral ageing by following apatitic OH^- , labile PO_4^{3-} or H_2O evolutions. This study will contribute to an enhanced control of young bone mineral dynamism and improvement of NHA-based orthopedic and dental biomaterials bioactivity.

Keywords: Biomimetic apatite; maturation process; labile-phosphate roles; hydroxylation, microstructural properties.

1. Introduction

The vertebrate's hard-calcified tissue (bone and teeth) is described as an organo-mineral composite. The mineral phase is identified as nano-sized hydrated apatites (NHA) [1-3]. They play an important role in both the bio-mineralization and the high dynamism of bone. which is constantly remodeling to adapt to the mechanical stresses and the storage of ions, in particular calcium and phosphate, to be removed for the mineral metabolic regulation (homeostasis) [4]. Thus, the synthetic NHA, having comparable characteristics as well as similar behaviors to those of bioapatites, are recognized as biomimetic material. They are widely used as potential bioactive substitutes in reconstructive, orthopedic and dental surgery [5]. Stœchiometric hydroxyapatite (HA), having of hexagonal structure with P63/m space group and specific composition $\text{Ca}_{10}(\text{PO}_4)_6(\text{OH})_2$, with both Ca/P and OH/P atomic ratios 1.67 and 0.33 respectively, is commonly regarded as a basic product of the bioapatites [2]. They are commonly described as poorly crystallized Ca-deficient NHA with atomic Ca/P ratio ranging from 1.33 to less than 1.67. This non stœchiometry is mainly related to the substitution of PO_4^{3-} ions by bivalent ones like HPO_4^{2-} and CO_3^{2-} . In this case, the loss of negative charge will be compensated by vacancies in calcium or OH^- sites. At the first stage, biological and synthetic NHA have similar composition, and they are poorly carbonated and non-hydroxylated [6-8]. The important characteristics of biological and synthetic HNA's nanocrystals compared to those large crystals (as for HA), are that the outer surfaces of a single crystal grain have been built by broken bonds called by surface unit-cells, which create strong distortions of the underlying

atomic arrangement transforming them into strained edge. Thus, the apatitic domains would be described as formed by the complete core unit cells surrounded by the incomplete surface ones which are in interaction with water molecules [7,9]. These latter are located in the surface shells with 1–2 nm deep [10,11]. The composition and structure of the hydrated shells are different from those apatitic domains [9,12,13]. The main orthophosphate groups building the apatitic tri-dimensional domains are the trivalent PO_4^{3-} ions. In contrast, the hydrated layers are described to be bi-dimensional structured in wet samples but amorphous in dried ones [9-14]. Besides, in the hydrated shells, which encompass between 44-55% of total phosphorus, the HPO_4^{2-} bivalents species are predominant if the synthesis pH is closer to the physiological value [9,15]. The specific behavior of the hydrated shell entities is certainly that these latter have high mobility and fast reversible exchange ability with the surrounding liquid environment [9,16]. Hence, these non apatitic species are commonly designed as labile ones. Spectroscopic investigations (XANES, FTIR and MAS NMR...) have established the presence of mostly labile bivalents ions, having specific spectral features, as Ca^{2+} , HPO_4^{2-} , PO_4^{3-} and/or CO_3^{2-} , closed to water molecules [12,14,17-20]. Similarity of chemical behavior between labile HPO_4^{2-} and Ca^{2+} demonstrates that they share the same environments and might be connected with low energy hydrogen bonds [15]. The ability of NHA to evolve in aqueous media in bone-like mineral with age (maturation) has interested several authors who investigated various routes for a better understanding of the maturation process of the biomimetic apatites as well as the biological ones [6,21-24]. The maturation is manifested by different evolutions such as the alteration of labile entities and hydration water, the changes in microstructural features or in apatitic hydroxyl ions content from NHA nascent crystals to aged ones. Some authors mainly focused on the labile species evolution, water alteration and/or hydroxyl ions change have been carried out. While other searches claimed that the labile species are difficult to interpret in mechanistic sense; they were interested in changes in microstructural behaviors of the NHA's crystals. Rey and co-workers have proposed through studies on NHA analogous to bone mineral (biomimetic apatites), that HP^{L} entities can interact to produce apatitic phosphate groups incorporated into surface apatitic cells in the growing apatites [9, 25]. Although this interesting discovery is crucial to understand how the HP^{L} ions control apatite ageing, some aspects are not clarified, such as (i) the role of labile trivalent phosphate ions and (ii) if the labile orthophosphate entities play some role in the fact that immature bioapatites are not hydroxylated at the earliest age. The lack of OH^- ions in the nascent nanocrystals of biological or biomimetic apatites is observed in opposition to that in the aged ones [6,8,26-28]. Different attempts have been advanced to explain the evolution of the OH^- content with ageing using different methods [6-8,29]. Certain authors suggested that OH^- groups are present in the apatite but they are not detected by FTIR or ^1H NMR spectroscopy because of the spectacular broadening of the spectra, which is due to the NHA's crystals microstructural features (the very small size, the poor crystallinity and the distortion in the lattice). Moreover, Blumenthal *et al.* have suggested that this absence is due to hydrogen bonding of hydroxyl groups with water [6]. Recently, Pajchel *et al.* have confirmed that the amount of structural OH^- groups in nanocrystalline apatites decreases with both the decreasing crystal size and the increasing of structural disorder, in accordance with Wopenka and Pasteris' idea [7,8,29]. They proposed that the structural disorder prevents the incorporation of the structural hydroxyl groups. They stated that the adsorbed water molecules are capable of moving from the hydrated shells surrounding surface crystallites into the lattice c-axis channels of apatite, this process introduced considerable structural disorders around and within those channels which discriminate the incorporation of OH^- ions. These controversies in the literature are probably due to the fact that the authors in these previous studies have not taken into account the evolutions of all chemical and structural nanocrystals characteristics at the same time. According to the available references in literature, no comprehensive study has been conducted on biomimetic apatite and has taken into consideration the evolution of all physicochemical parameters during maturation, as it is difficult to assess the continuous and the complex events during maturation in particular at an early age.

The current investigation is aimed at studying the evolution of all parameters of NHA crystals in order to have a better understanding of maturation process of bioapatites at early age. Our attempt is to explain: (i) how the hydrated shell constituent alteration contributes to the building of the apatitic species especially the role of labile PO_4^{3-} that has been neglected in the former proposed maturation process and (ii) why the OH^- ions are not detected in NHA's nascent nanocrystals as in young bone mineral. For that purpose, we want to identify, using statistical treatment, if there are any possible significant relationships between hydrated shell entities (as explaining variables) and apatitic species or physical features (as explained variables).

In order to achieve this, we have adopted the following annotations for the used variables as shown in the abbreviation list below:

Ca/P:	Molar atomic ratio	I_{cr} :	Crystallinity index	n_{H_2O} :	Number of water moles
Ca^L :	Labile calcium	I_M :	Mineral maturity index	OH^{ap} :	Apatitic OH
HP^{ap} :	Apatitic HPO_4^{2-}	L_a :	Apparent size along a-axis	OH^L :	Labile OH
HP^L :	Labile HPO_4^{2-}	L_c :	Apparent size along c-axis	PO^{ap} :	Apatitic PO_4^{3-}
PO^L :	Labile PO_4^{3-}	ε :	Distorsion index	$\Delta_{sol} H_{298}^\circ$:	Standard enthalpy of dissolution at 298K

2. Materials and techniques

2.1. Elaboration

Poorly crystalline apatites were synthesized by double decomposition method in phosphate-buffered solution which allows the pH to stabilize around the physiological value (7.35 ± 0.05) [30]. A calcium nitrate solution (17.7 g $Ca(NO_3)_2 \cdot 4H_2O$ in 0.250 L of deionised water) was rapidly poured into an ammonium phosphate solution (40 g of $(NH_4)_2HPO_4$ in 0.500 L of deionized water). The suspensions were left to mature, without stirring, at an ambient temperature for variable periods of time namely 1/3 hour (h), 1 h, 3 h, 6 h, 12 h, 1 day (d), 3 d, 15 d, 1 month (m) and 6 m. They were stocked in hermetically closed flasks to prevent water evaporation and minimize carbonate uptake from the atmosphere. Then, they were filtered through a Buchner funnel and washed with deionized water. The obtained gel samples were lyophilized in the same conditions (during 72 h; Heto[®] CT60c). All powder samples were stored in a freezer at 255 K to avoid any spontaneous transformation between experiments.

2.2. Physico-chemical methods

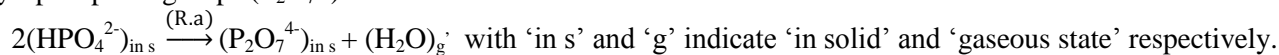
All samples were analyzed by PANalytical X'pert pro MPD[®] powder diffractometer in Bragg-Brentano geometry. The XRD patterns were collected using $Cu_{K\alpha}$ radiation ($\lambda = 1.5406 \text{ \AA}$) in the range of $2\theta = 20-70^\circ$ with a step size of 0.0167° and a counting time of 1300 s per step. The patterns are used to identify crystalline phases and also to evaluate both their micro structural and micro textural parameters. The apparent size of the crystals along *c*-axis (L_c) or *a*-axis (L_a) was reached by measuring the (002) or (310) line broadening at half of the maximum intensity (FWHM) using Scherrer's formula:

$$L_{\perp(hkl)} = \frac{0.9 \lambda}{\cos(\theta_{(hkl)}) \sqrt{\Delta_R^2 - \Delta_0^2}}$$

where $L_{\perp(hkl)}$ is the mean size of the ordered micro-domains in direction perpendicular to (hkl), 0.9 is a dimensionless shape factor used for apatite, λ is the X-ray wavelength; $\theta_{(hkl)}$ is the Bragg angle of (hkl) line, Δ_R and Δ_0 are the width of the (hkl) lines of the studied sample and well crystallized HA respectively.

Fourier Transformed Infra-Red spectroscopy is a current method to identify and to control the purity of the solid phase as well as to quantify labile and apatitic species amount [30]. For all samples, the characterization has been carried out three times on the lyophilized powder. IR spectra are recorded with absorbance mode on FTIR spectrophotometer (Perkin-Elmer FTIR1600[®]) from KBr pellets (1-3 mg of sample per 300 mg of KBr).

Calcium amount was determined by complexometry with ethylenediaminetetraacetic acid [31]. The total-phosphorus and the HPO_4^{2-} content were analyzed by colorimetry according to the protocol proposed by Gee and Dietz [32]. The samples were heated at 873 K during one hour to convert the HPO_4^{2-} ions into pyrophosphate groups ($P_2O_7^{4-}$) with the release of water as the follow reaction scheme:



Then, UV-visible spectrophotometry (JENWAY[®] 6400) of the phosphovanado-molybdic acid was performed, before and after the hydrolysis of the pyrophosphate moiety by boiling with nitric acid, at 460 nm.

Thermal gravimetric analysis was carried out with Toledo TGA/DTA 851e[®] equipment. A precise mass of the sample to be analyzed $\sim 20.0 (\pm 0.2)$ mg was put in 150 μ L platinum crucibles. The TG-loss recorded between ambient temperature and 773 K from which is subtracted the quantity of water associated to the condensing of HPO_4^{2-} ions of the NHA (R.a) enable us to quantify hydration water. Mg^{2+} content, which could be present in traces in the commercial initial reagents, was analyzed by atomic absorption spectroscopy [33]. For each sample, OH ion content was calculated considering the ionic charge electro neutrality to establish its chemical formula.

2.3. Calorimetry

The measurement of the standard enthalpy of dissolution of each sample, in 10w% nitric acid solution was performed in Tian-Calvet heat-flux microcalorimeter (C-80 SETERAM[®]), at 298 K. The calorimetric experimental procedure was described in detail in previous work [34].

3. Results

3.1. Collected data

3.1.1. Structural and textural characteristics

- XRD analysis:

X-ray diffractograms of all samples lead to similar results. They have broad lines which are characteristic of a poorly crystallized phosphate apatite, without the presence of other foreign crystalline phase (Fig. 1). The considerable broadening of the XRD lines is due to various types of micro-structural details. Among these, we can mention the small crystallite size of the coherently diffracting domains as well as the increasing disorder and lattice strains (distortions) within the crystals [35]. All samples show an elongation along the *c*-axis as usually found for bioapatites [10,30]. Weak increase and no significant changes of the apparent sizes L_c and L_a respectively were observed at the earliest stage until 1 day of ageing. After that, a fast increase of each parameter is detected until one month and then it becomes slowly (Fig. 2).

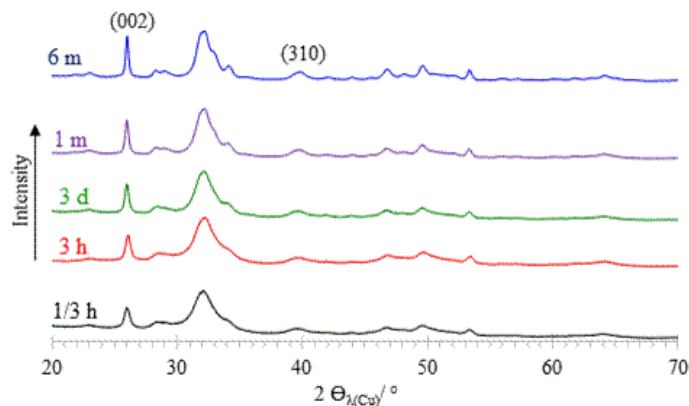


Figure 1: Evolution of DRX diffractograms with maturation time, where: h, d and m are hour(s), days and month(s) respectively.

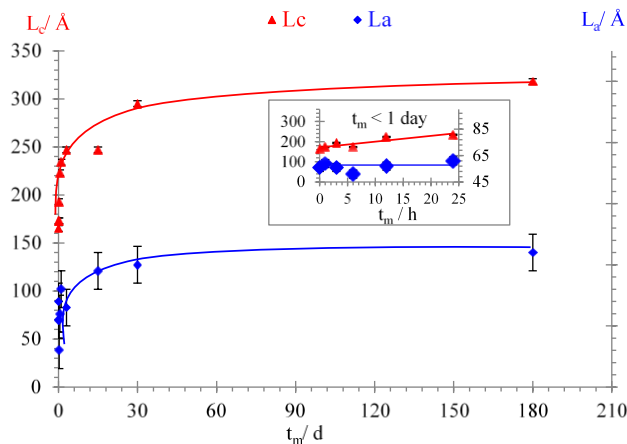


Figure 2: Evolution of apparent lattice parameters L_c and L_a with NHA's maturation time.

Mineral crystallinity index (I_{cr}) is defined as the degree of crystallinity, corresponding to the fraction of crystalline phase present in the examined volume [36]. It was evaluated using the following equation:

$$I_{cr} = \left(\frac{0.24}{\Delta_{002}} \right)^3, \text{ where: } \Delta_{002} \text{ is FWHM } (^\circ) \text{ of } (002) \text{ reflection.}$$

The apparent distortion index (ϵ) of a crystal lattice is the amount of the variation of spacing within (or possibly between) domains. It is caused by the elevated density of defects with long range stress fields. It was calculated by Stokes and Wilson's formula [35,37]: $\epsilon = \frac{\beta}{4 \tan \theta_{(002)}}$, where: β is the integral breadth of the Gaussian component and $\theta_{(002)}$ is the Bragg angle of reflection (002). The curves of the evolutions of these two parameters with maturation time are superimposed, as in Figure 3. These parameters appear in correlation: when I_{cr} increases progressively, ϵ decreases in the same pattern. Up to 1 day, weak evolution is observed. These changes are quicker until 1 month. Then, they slow down to reach about 0.4 and 0.01 level for I_{cr} and ϵ respectively after 6 months of ageing.

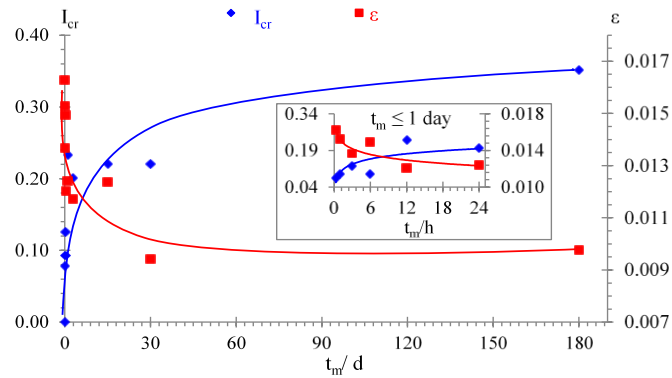


Figure 3: Evolution of crystallinity index (I_{cr}) and micro-strain apparent coefficient (ϵ) with NHA's maturation time.

- FTIR spectroscopy data:

FTIR spectra of the all samples are characteristic of poorly crystallized hydrated hydroxyapatite free of carbonate (Fig. 4.A). They are dominated by both poorly resolved broad bands assigned to $\nu_4\nu_2\text{PO}_4^{3-}$ ($700\text{-}400\text{ cm}^{-1}$) and $\nu_3\nu_1\text{PO}_4^{3-}$ ($1200\text{-}900\text{ cm}^{-1}$) domains as well as water molecules bands in the OH stretching domain ($3400\text{-}3000$) and in HOH deformation domain (1630 cm^{-1}). The weak band at 870 cm^{-1} generated by HPO_4^{2-} ions is observed in all spectra. The two bands assigned to apatitic OH^- liberation and stretching vibrations are exhibited at 630 cm^{-1} and 3565 cm^{-1} only after 1 and 3 days respectively. The poorly resolved spectra indicate the low rate of crystallization as shown by XRD data. In order to get a more precise evaluation of the structural characteristic of the NHA's crystals during maturation, $\nu_4\nu_2\text{PO}_4^{3-}$ IR-domain was deeply studied using Fityk[®] software. After baseline correction and normalization at absorbance 1 on the $\nu_3\nu_1\text{PO}_4^{3-}$, the curve fitting of an individual spectrum was performed. This spectral domain was decomposed into eight elementary bands (Fig. 4.B), according to previous studies [38, 39].

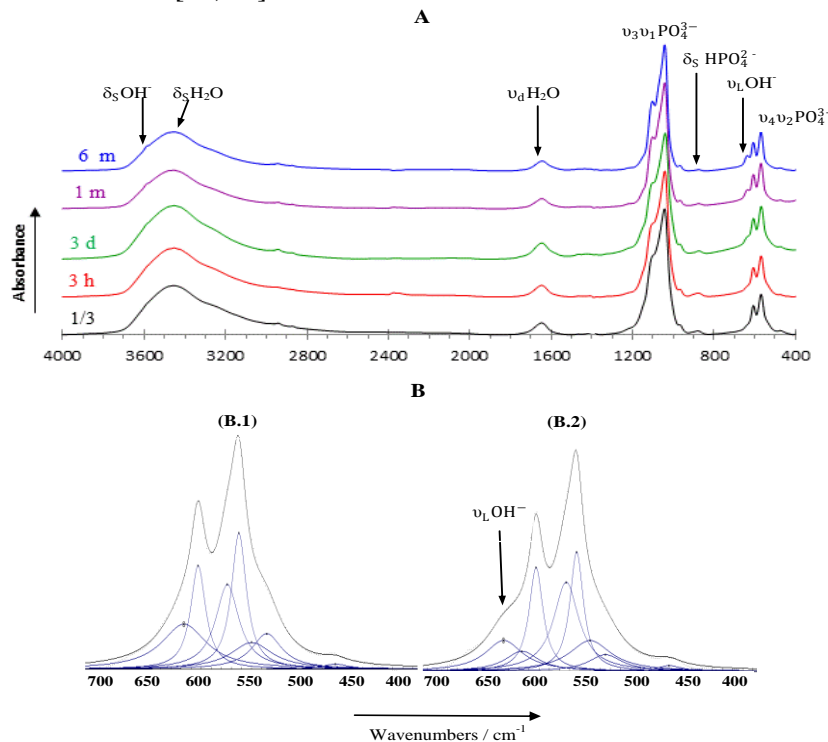


Figure 4: FTIR spectra: A: Evolution with maturation time, where: h, d and m are hour(s), days and month(s) respectively; B: Decomposition of the $\nu_4\nu_2(\text{PO}_4^{3-})$ IR domain: (B.1) NHA's nascent nanocrystals ageing up to 1 day (3 h) and (B.2) NHA's ageing at 1 day, showing: non-apatitic HPO_4^{2-} (535 cm^{-1}), non-apatitic PO_4^{3-} (617 cm^{-1}), apatitic PO_4^{3-} ($601, 575$ and 560 cm^{-1}), apatitic OH^- (630 cm^{-1}) and apatitic HPO_4^{2-} (550 cm^{-1}).

The output of this analysis was expressed as relative intensity of the elementary band to the sum of the areas of the components assigned to the orthophosphate species. Thus, the amounts of HP^L , PO^L , PO^{ap} , OH^{ap} and HP^{ap} were determined. For each sample, the decomposition was realized on the three recorded spectra. The average

values of the labile and apatitic species content are shown in Figures 5 and 6. They indicate that the earliest immature apatites (up to 1 day) are the richest in labile orthophosphate groups especially the HP^L entities. With ageing, the increase of PO^{ap} , OH^{ap} and HP^{ap} content are observed instead of the deterioration of labile orthophosphate entities. However, although the labile entities have the same fate, some important differences in behavior are revealed: until about 1 day, there is a decrease of HP^L species and an increase of PO^{ap} ones (Fig. 5) without significant change of HP^{ap} , PO^L and OH^{ap} species (Fig. 6). After the first day of the ageing, significant changes are observed: an increase of the apatitic entities (PO^{ap} , HP^{ap} and OH^{ap}) at the expense of the decrease of labile groups (HP^L and PO^L).

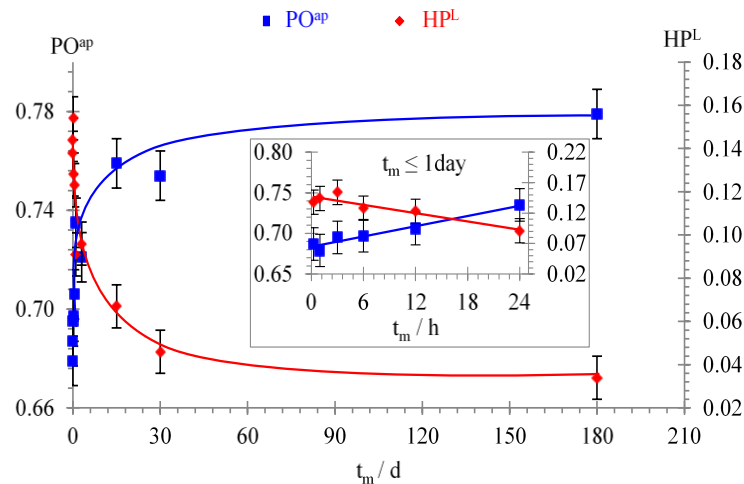


Figure 5: Changes of the labile HPO_4^{2-} (HP^L) species amount and the apatitic PO_4^{3-} (PO^{ap}) one with NHA's maturation time.

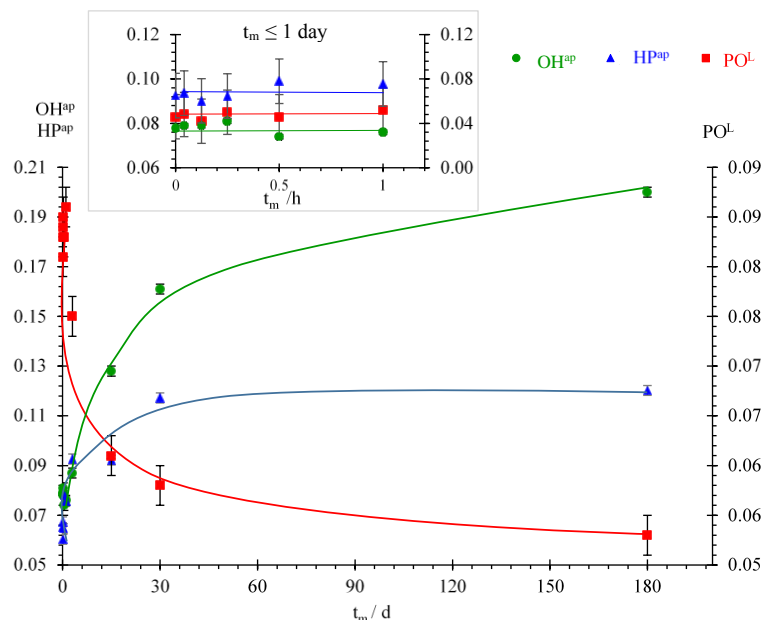


Figure 6: Changes of the labile PO_4^{3-} (PO^L) group amount and HPO_4^{2-} (HP^{ap}) and OH (OH^{ap}) species ones with NHA's maturation time.

Besides, to follow the progressive transformation of non apatitic domains into poorly then well crystallized apatite, the mineral maturity index (I_M) is measured using the following equation:

$$I_M = \frac{A_{550}^{HP^{ap}} + (A_{560}^{PO^{ap}} + A_{575}^{PO^{ap}} + A_{601}^{PO^{ap}})}{A_{535}^{HP^L} + A_{617}^{PO^L}}$$

where: A_{ν}^i is the area of the FTIR band of the orthophosphate entity "i" at specific wavenumber (ν). The I_M continuously evolves with the maturation time (Fig.7).

3.1.2. Calorimetric analysis

Standard enthalpy of NHA's dissolution at 298 K becomes more negative when the maturation time increases (Fig. 7). This result indicates that the NHA are more stable with ageing [25,34]. The continuous profile of the evolution of the enthalpy with time is reminiscent of the continuous profile of the maturity index: they change rapidly, but inversely.

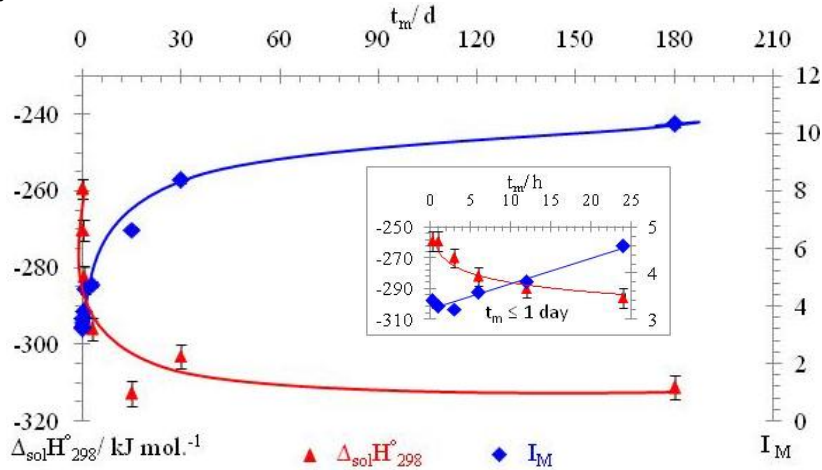
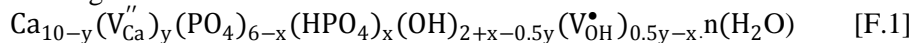


Figure 7: Continuous changes of NHA's standard dissolution enthalpy at 298 K ($\Delta_{\text{sol}}H^{\circ}_{298}$) and the maturity index (I_M), with maturation time.

3.1.3. Chemical analysis

The data collected by chemical and thermo gravimetric analysis reveal that the samples are Ca-deficient hydrated apatite having as chemical formula:



Where: V_{Ca}'' and $\text{V}_{\text{OH}}^{\bullet}$ are the Ca^{2+} and OH^- ion vacancies respectively, as $0.28 \leq y \leq 1.54$, $0.48 \leq x \leq 1.26$ and $4.33 \leq n \leq 7.76 \text{ H}_2\text{O mol}$.

During maturation, the Ca/P atomic ratio increases whereas the HP/P atomic ratio decreases with logarithmic continuous profile, without a significant change of the hydrated shell water content (Fig.8). After 1 day, with the release of hydration water, the changes of two atomic ratios become slow, towards stoichiometry. Added to that, the prepared samples contain less than 0.1% of Mg^{2+} ions which are known as a crystallization inhibitor species. The presence of such trace cannot have significant effects on the apatite growth [40].

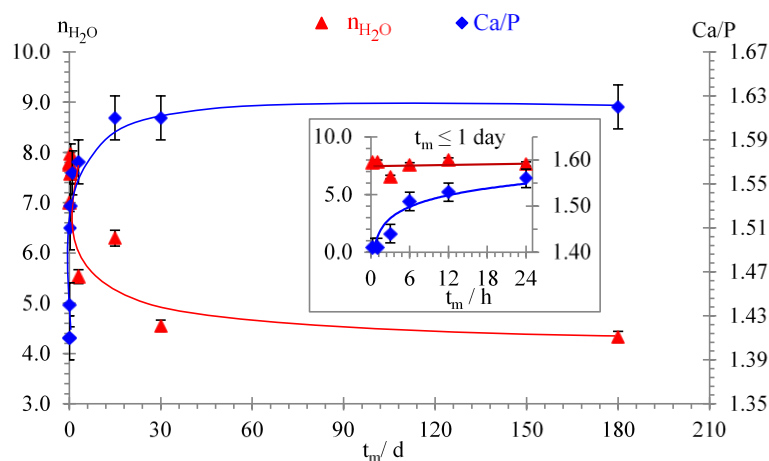


Figure 8: Evolution of Ca/P atomic ratio and the number of $\text{H}_2\text{O mol}$. with NHA's maturation time.

3.2. Statistical analysis

3.2.1. Data sets organization

In these experimental conditions, the maturation time can be divided into two periods based on the profile of the parameter's evolution. During the earliest period of the NHA's maturation (up 1 day), a first kind of parameters is characterized by fast changes while a second kind has no significant change. Nevertheless, during the last

period (beyond 1 day), all NHA's characteristics evolve around those of the stoichiometric hydroxyapatite. The first category gathers the following parameters: HP^L , PO^{ap} , Ca/P , $\Delta_{sol} H_{298K}^\circ$ and I_M ; whereas the second one groups the remaining NHA characteristics (PO^L , HP^{ap} , OH^{ap} , n_{H_2O} , L_c , L_a , I_{cr} and ϵ). Accordingly, we have carried out a statistical study of three periods successively: the earliest short period, the last long one and the entire maturation study time. The preliminary organization of the data sets of the explained and explaining variable pairs studied is presented in Table 1.

3.2.2. Statistical Model choice

In this study, we have been more interested in the exploratory statistical analysis of the data to highlight which hydrated shell species is correlated with the other parameters and how. Thus, we have been concerned only with establishing "robust" (*i.e.* well-defined) relationships in the data, precise measures of prediction are not our concern. Therefore, the small sample sizes of both the earliest and last maturation periods are not crucial here. They will result in an enlargement of confidence interval. Besides, the realization of the multiple linear regressions, where the parameters are estimated using ordinary least squares method, is authorized if all the explaining variables are independent pair wise [41]. Multicollinearity can cause serious instabilities on some estimators. Erkel-Rousse indicates that in an ordinary linear model affected by multicollinearity, the estimators remain without the optimal linear bias, and it has the disadvantage of being low robust.

In order to avoid the effect of the multicollinearity, the Simplified Alternative Regression Method (OLSM: Ordinary List squares Method) can be applied, without prejudice, if the number of the predictors (N) is not important [42]. OLSM consists in estimating all possible univariate combinations between explained variables and explaining ones (*i.e.* 2^{N-1} possibilities). Thus, the OLSM's aim is to fit a 'best' straight line of the equation form hereinafter to a set of n data pairs $\{X_{k,i}, Y_i\}$: $Y_i = \beta_{0,i} + \beta_{1,i} X_{k,i} + \mu_{k,i}$ where, $\beta_{0,i}$ and $\beta_{1,i}$ are the regression coefficients. The model assumes that their deviations $\mu_{k,i}$ from the line are normally distributed with means zero and constant variances ($\mu_{k,i}^2$). To predict what variables among shell's constituents control on apatite characteristics during ageing, the null hypothesis H_0 is that each explaining variable (labile ions or water) has absolutely no influence (no correlation) on the explained one of each pair ($X_{i,k}$, Y_i).

Table 1: Organization of the data set of the variable pairs studied ($X_{k,i}$, Y_i): explained variables (Y_i) with the possible control variables ($X_{k,i}$).

Variables	Correlation of the apatitic entities with the labile species and water	Correlation of the physical feature with the labile species and water
Y_i	PO^{ap} , $\frac{Ca}{P}$, $HP^{ap^{(c)}}$ and/or $OH^{ap^{(c)}}$	$\Delta_{sol} H_{298K}^\circ$, I_M , I_{cr} , L_c , $L_a^{(c)}$ and/or ϵ
$X_{k,i}$	HP^L , $PO^{L^{(c)}}$ and/or $n_{H_2O}^{(c)}$	

^(c)No significant change has been observed during the earliest period (up to 1 day).

3.2.3. Statistical treatment

In this study, all variables are normally distributed according to Kolmogorov-Smirnov's test. The applied process has at most the following successive steps: (1) Correlation coefficient determination; (2) Correlation significance and (3) Regression estimation [42-46]. Statistical analyses were performed using the software IBM SPSS 20[®]. The successive steps described in the appendix were applied to check the linear correlation between the pair variables ($X_{i,k}$, Y_i) for both the earliest and last periods. According to the collected data, only when the evolution is continuous for a two periods, the linear relationship is tested for the entire maturation.

3.2.4. Statistical data

Correlation coefficient and significant linear regressions data between hydrated shell entities and apatitic species are grouped in Table 2. It demonstrates that the selected regression equation slope signs are in coherence with the observed experimental evolutions. Hydrated shell constituents are negatively correlated to the apatitic species through significant linear regressions. During the two periods and the entire maturation time, among the three explaining variables, only HP^L changes have strong negative correlations and significant relationships with the PO^{ap} species and Ca/P ratio. However, during the second period, HP^L is strongly negatively associated, with the remaining explained variables, except the dissolution enthalpy. In contrast, PO^L and H_2O have correlations only in the second period of maturation. In fact, up to water release, the slow decrease of PO^L species has strong correlations with the increase of PO^{ap} , Ca/P ratio, HP^{ap} and OH^{ap} , whereas, H_2O is negatively strongly correlated

only to HP^{ap} and OH^{ap} . The correlations between labile, water and physical characteristics of NHA are presented in Table 3. Microstructural lattice parameters of NHA nanocrystals have no correlations with the explaining variables in the first period. Paradoxically, in the second period L_c and I_{cr} have strong and significant negative correlations with all the explaining variables, whereas, L_a is negatively correlated to both HP^L and PO^L . Moreover, the micro-strain coefficient change is only explained by HP^L alteration. The enthalpy of dissolution and maturity index are correlated in the first period to HP^L while in the second period, maturity index has strong correlations with all the explaining variables but $\Delta_{sol} H_{298K}^\circ$ is positively correlated only with H_2O change.

Table 2: Correlation coefficient ($r_{X_{k,i}, Y_i}^{Period}$) and significant univariate linear regression, between apatitic species amount and Ca/P atomic ratio (Y_i as explained variable) and hydrated shell entity quantity ($X_{k,i}$ as explaining variable), during the first (I), the second (II) and the entire (t) periods of NHA's maturation.

Variables		Period of maturation time		
Y_i (i)	$X_{k,i}$ (k)	1 st period (Earliest) (½ h - 1 day)	2 nd period (last) (1 day - 6 months)	Entire maturation time (½ h - 6 months)
PO^{ap} (1)	HP^L (1)	$[E_{1,1}^I]$ $PO^{ap} = 0.803 - 0.797 HP^L$ ($p < 0.01$) ^(a) $r_{1,1}^I = -0.896, R^2 = 0.803; s = 0.01$ ^(b)	$[E_{1,1}^{II}]$ $PO^{ap} = 0.80 - 0.76 HP^L$ ($p < 0.01$) $r_{1,1}^{II} = -0.923, R^2 = 0.852; s = 0.01$	$[E_{1,1}^t]$ $PO^{ap} = 0.801 - 0.78 HP^L$ ($p < 0.01$) $r_{1,1}^t = -0.968, R^2 = 0.938; s = 0.01$
	PO^L (2)	$r_{2,1}^I = 0.519$ n-Sig Corr ^(a)	$[E_{2,1}^{II}]$ $PO^{ap} = 0.84 - 1.38 PO^L$ ($p < 0.1$) $r_{2,1}^{II} = -0.834, R^2 = 0.696; s = 0.01$	No calculated
	n_{H_2O} (3)	$r_{3,1}^I = 0.403$ n-Sig Corr	$r_{3,1}^{II} = -0.531$ n-Sig Corr	
$\frac{Ca}{P}$ (2)	HP^L (1)	$[E_{1,2}^I]$ $\frac{Ca}{P} = 1.80 - 2.50 HP^L$ ($p < 0.05$) $r_{1,2}^I = -0.846, R^2 = 0.716; s = 0.04$	$[E_{1,2}^{II}]$ $\frac{Ca}{P} = 1.66 - 0.92 HP^L$ ($p < 0.05$) $r_{1,2}^{II} = -0.922, R^2 = 0.851; s = 0.03$	$[E_{1,2}^t]$ $\frac{Ca}{P} = 1.71 - 1.78 HP^L$ ($p < 0.01$) $r_{1,2}^t = -0.915, R^2 = 0.838; s = 0.04$
	PO^L (2)	$r_{2,2}^I = 0.568$ n-Sig Corr ^(c)	$[E_{2,2}^{II}]$ $\frac{Ca}{P} = 1.72 - 1.956 PO^L$ ($p < 0.01$) $r_{2,2}^{II} = 0.983, R^2 = 0.966; s = 0.01$	No calculated
	n_{H_2O} (3)	$r_{3,2}^I = 0.228$ H_0 n-Rej ^(d)	$r_{3,2}^{II} = -0.726$ n-Sig Corr	
HP^{ap} (3)	HP^L (1)	$r_{1,3}^I = -0.762$ n-Sig Corr	$[E_{1,3}^{II}]$ $HP^{ap} = 0.14 - 0.61 HP^L$ ($p < 0.05$) $r_{1,3}^{II} = -0.892, R^2 = 0.795; s = 0.01$	$[E_{1,3}^t]$ $HP^{ap} = 0.13 - 0.49 HP^L$ ($p < 0.01$) $r_{1,3}^t = -0.950, R^2 = 0.903; s = 0.01$
	PO^L (2)	$r_{2,3}^I = -0.568$ n-Sig Corr	$[E_{2,3}^{II}]$ $HP^{ap} = 0.18 - 1.22 PO^L$ ($p < 0.05$) $r_{2,3}^{II} = -0.891, R^2 = 0.794; s = 0.01$	No calculated
	n_{H_2O} (3)	$r_{3,3}^I = -0.675$ n-Sig Corr	$[E_{3,3}^{II}]$ $HP^{ap} = 0.174 - 0.013 n_{H_2O}$ ($p < 0.05$) $r_{3,3}^{II} = -0.966, R^2 = 0.933; s = 0.01$	
OH^{ap} (4)	HP^L (1)	$r_{1,4}^I = -0.505$ n-Sig Corr	$[E_{1,4}^{II}]$ $OH^{ap} = 0.25 - 1.87 HP^L$ ($p < 0.01$) $r_{1,4}^{II} = -0.983, R^2 = 0.967; s = 0.01$	No calculated
	PO^L (2)	$r_{2,4}^I = -0.015$ H_0 n-Rej	$[E_{2,4}^{II}]$ $OH^{ap} = 0.37 - 3.55 PO^L$ ($p < 0.05$) $r_{2,4}^{II} = -0.934, R^2 = 0.873; s = 0.02$	No calculated
	n_{H_2O} (3)	$r_{3,4}^I = -0.402$ n-Sig Corr	$[E_{3,4}^{II}]$ $OH^{ap} = 0.31 - 0.03 n_{H_2O}$ ($p < 0.1$) $r_{3,4}^{II} = -0.823, R^2 = 0.678; s = 0.03$	

(a) p: Probability of the obtaining observed effect under a null hypothesis (H_0).
 (b) R^2 : Determination coefficient and s: Standard error of the univariate linear regression.
 (c) n-Sig Corr: No significant correlation.
 (d) H_0 n-Rej: Hypothesis H_0 no-rejected.

Table 3: Correlation coefficient ($r_{X_{k,i}, Y_i}^{\text{Period}}$) and significant univariate linear regression, between the nanocrystals physical features (Y_i as explained variable) and hydrated shell entity amount ($X_{k,i}$ as explaining variable), during the first (I), the second (II) and the entire (t) periods of NHA's maturation.

Variables		Maturation time period		
Y_i (i)	$X_{k,i}$ (k)	1 st period (Earliest) ($\frac{1}{3}$ h-1 day)	2 nd period (last) (1 day-6 months)	Entire maturation time ($\frac{1}{3}$ h-6 months)
I_M (5)	HP ^L (1)	$[E_{1,5}^I]$ $I_M = 6.6 - 22.9 \text{ HP}^L$ ($p < 0.05$) $r_{1,5}^I = -0.995, R^2 = 0.989; s = 0.06^{(a)}$	$[E_{1,5}^{II}]$ $I_M = 12.46 - 83.89 \text{ HP}^L$ ($p < 0.05$) $r_{1,5}^{II} = -0.949, R^2 = 0.901; s = 0.87$	$[E_{1,5}^t]$ $I_M = 10.86 - 55.47 \text{ HP}^L$ ($p < 0.05$) $r_{1,5}^t = -0.950, R^2 = 0.903; s = 0.87$
	PO ^L (2)	$r_{2,5}^I = 0.776$ n-Sig Corr ^(b)	$[E_{2,5}^{II}]$ $I_M = 17.05 - 153.11 \text{ PO}^L$ ($p < 0.1$) $r_{2,5}^{II} = -0.867, R^2 = 0.751; s = 1.38$	No calculated
	n _{H2O} (3)	$r_{3,5}^I = 0.408$ n-Sig Corr	$[E_{3,5}^{II}]$ $I_M = 15.27 - 1.48 \text{ n}_{H_2O}$ ($p < 0.1$) $r_{3,5}^{II} = -0.841, R^2 = 0.707; s = 1.50$	
$\Delta_{sol} H_{298}^\circ$ (6)	HP ^L (1)	$[E_{1,6}^I]$ $\Delta_{sol} H_{298}^\circ = -351 + 577 \text{ HP}^L$ ($p < 0.05$) $r_{1,6}^I = 0.812, R^2 = 0.659; s = 10$	$r_{1,6}^{II} = 0.612$ n-Sig Corr	
	PO ^L (2)	$r_{2,6}^I = 0.487$ n-Sig Corr	$r_{2,6}^{II} = 0.711$ n-Sig Corr	No calculated
	n _{H2O} (3)	$r_{3,6}^I = 0.152$ H ₀ n-Rej ^(c)	$\Delta_{sol} H_{298}^\circ = -345.3 + 6.5 \text{ n}_{H_2O}$ ($p < 0.05$) $r_{3,6}^{II} = 0.938, R^2 = 0.880; s = 3.8$	
L_c (7)	HP ^L (1)	$r_{1,7}^I = -0.717$ n-Sig Corr	$[E_{1,7}^{II}]$ $L_c = 351 - 1236 \text{ HP}^L$ ($p < 0.05$) $r_{1,7}^{II} = -0.924, R^2 = 0.855; s = 6$	
	PO ^L (2)	$r_{2,7}^I = 0.241$ H ₀ n-Rej	$[E_{2,7}^{II}]$ $L_c = 415.5 - 2211.9 \text{ PO}^L$ ($p < 0.1$) $r_{2,7}^{II} = -0.828, R^2 = 0.685; s = 23.5$	No calculated
	n _{H2O} (3)	$r_{3,7}^I = 0.072$ H ₀ n-Rej	$[E_{3,7}^{II}]$ $L_c = 402.5 - 23.7 \text{ n}_{H_2O}$ ($p < 0.05$) $r_{3,7}^{II} = -0.886, R^2 = 0.786; s = 19.4$	
L_a (8)	HP ^L (1)	$r_{1,8}^I = -0.407$ n-Sig Corr	$[E_{1,8}^{II}]$ $L_a = 71.3 - 124.5 \text{ HP}^L$ ($p < 0.05$) $r_{1,8}^{II} = -0.956, R^2 = 0.914; s = 1.2$	
	PO ^L (2)	$r_{2,8}^I = 0.180$ H ₀ n-Rej	$[E_{2,8}^{II}]$ $L_a = 77.27 - 214.32 \text{ PO}^L$ ($p < 0.1$) $r_{2,8}^{II} = -0.823, R^2 = 0.677; s = 2.3$	No calculated
	n _{H2O} (3)	$r_{3,8}^I = 0.180$ H ₀ n-Rej	$r_{3,8}^{II} = -0.532$ n-Sig Corr	
I_{cr} (9)	HP ^L (1)	$r_{1,9}^I = -0.721$ n-Sig Corr	$[E_{1,9}^{II}]$ $I_{cr} = 0.48 - 2.30 \text{ HP}^L$ ($p < 0.05$) $r_{1,9}^{II} = -0.924, R^2 = 0.854; s = 0.04$	
	PO ^L (2)	$r_{2,9}^I = 0.240$ H ₀ n-Rej	$[E_{2,9}^{II}]$ $I_{cr} = 0.62 - 5.18 \text{ PO}^L$ ($p < 0.1$) $r_{2,9}^{II} = -0.805, R^2 = 0.648; s = 0.06$	No calculated
	n _{H2O} (3)	$r_{3,9}^I = 0.018$ H ₀ n-Rej	$[E_{3,9}^{II}]$ $I_{cr} = 0.59 - 0.056 \text{ n}_{H_2O}$ ($p < 0.1$) $r_{3,9}^{II} = -0.871, R^2 = 0.755; s = 0.05$	
ϵ (10)	HP ^L (1)	$r_{1,10}^I = 0.653$ n-Sig Corr	$[E_{1,10}^{II}]$ $\epsilon = 0.008 + 0.043 \text{ HP}^L$ ($p < 0.1$) $r_{1,10}^{II} = 0.834, R^2 = 0.695; s = 0.001$	
	PO ^L (2)	$r_{2,10}^I = -0.205$ H ₀ n-Rej	$r_{2,10}^{II} = 0.690$ n-Sig Corr	No calculated
	n _{H2O} (3)	$r_{3,10}^I = -0.080$ H ₀ n-Rej	$r_{3,10}^{II} = 0.787$ n-Sig Corr	

(a), (b), (c) and (d) see notes under the Table 2.

Discussion

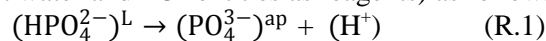
Both the elaboration and the ageing of the studied samples are performed in aqueous solution (Sol.) buffered by phosphate ions at pH = 7.35 and without foreign ions which could be trapped (e.g. Na⁺, F⁻ or CO₃²⁻) within solid phase. The freshly prepared NHA are rich in labile ions and water in agreement with previous works [8,9,14,15,17,23,29]. During maturation, the NHA are enriched with Ca²⁺ and apatitic ions (HP^{ap}, PO^{ap} and OH^{ap}) at the expense of the labile groups (HP^L and PO^L) depletion and the water loss. These evolutions lead to change in the microstructural characteristics of NHA's nanocrystals which become less reactive with age. Our findings reveal that the evolution of the NHA physical characteristics with ageing can be listed in two kinds, based on the similar curves profile. For both, the linear progression of each parameter is performed in two phases: the first occurs before the significant removal of water while the second phase is initiated simultaneously with dehydration. Several relationships between NHA's physicochemical features were reported, but to our knowledge, no one tried to estimate this correlation by univariate linear statistical method between (i) NHA's labile species and the apatitic environments (ii) NHA's labile species and the physicochemical features.

✓ How does hydrated shell constituent alteration contribute to the building of the apatitic domains?

To better understand the maturation process, we focus on both the correlation coefficient and the significant linear equations between the NHA's crystal hydrated shell's entities and the apatitic species (Table 2). During maturation, both the Ca/P ratio increase and the HP/P ratio decrease are observed simultaneously. Such changes can be explained by the increase of the Ca²⁺ amount, the decrease of the HPO₄²⁻ total content (HP^L and HP^{ap}), the increase of the total mole number of PO₄³⁻ (PO^L and PO^{ap}) or all of them in the apatite.

The present data show that the PO^{ap} generation is never associated with the water molecules change. However, the PO^{ap} formation is very strongly associated ($r_{1,1}^t = -0.968$, $p < 0.01$) with the disappearance of practically the equivalent of one mole of HP^L with the maturation time as shown in the following equation:

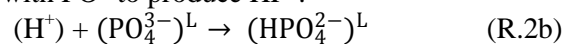
" $n_{PO^{ap}} = 4.81(\pm 0.02) - 0.79(\pm 0.16) n_{HP^L}$ ", which is equivalent to "6 x [E_{1,1}^t]" in order to convert the amount of PO^{ap} species to its mole number per apatite mole of which the building stability requires six moles of orthophosphate. Added to that, this chemical event occurs without the variation of both PO^L and HP^{ap} content, before the significant release of water. HP^L is still correlated with PO^{ap} even after that with respect to the same linear equations [E_{1,1}^I], [E_{1,1}^{II}] and [E_{1,1}^t]. Thus, we can deduce that the HP^L is converted into PO^{ap} during the entire maturation period (without water and PO^L entities as reagents) as follows:



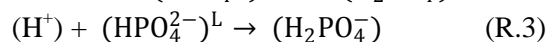
Free proton cannot stabilize in aqueous environment. Accordingly, it must bind quickly to the closest neighbouring negative or polar entities inside the hydrated layers. With respect to the mother solution composition, three possibilities could be proposed. The first proposal is that H⁺ entities interact with (OH⁻)^L ions as reagents to form water as following:



The second one is that H⁺ reacts with PO^L to produce HP^L:

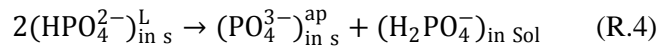


The third suggestion is that (H⁺) reacts with (HPO₄²⁻)^L into (H₂PO₄⁻) as the following reaction scheme shows:



The first assumption implies that with maturation time, the NHA water content increases and the NHA OH⁻ amount decreases (R.2a). What is observed is the opposite of what has been experimentally pointed out. In fact, IR spectra and TGA data as well as chemical formula (F.1) clearly indicate OH⁻ amount increase without any significant change of water content during the earliest time. We conclude that this assumption is rejected. Moreover, the second proposal (R.2b) is also rejected because it implies two opposite evolutions which are not observed in this period: PO^L decrease and HP^L increase. According to our results, only a decrease of HP^L, without PO^L significant change, is recorded. Then, we discuss the third proposal (R.3). To understand how the deficient apatites may interact with their natural surrounding solution (e.g. body fluid), Bengtsson and Sjöberg have studied the surface chemistry of deficient apatites, including not only solubility but also complexation in solution and in the mineral-water interface [47]. They established the distribution diagrams at 298 K showing surface speciation of deficient apatite in agreement with experimental data using several experimental methods (e.g. XPS, ³¹P NMR spectroscopy, zeta measurements...). This diagram predicts positively-charged ≡CaOH₂⁺ ('≡' stands for the surface) and negatively-charged ≡OPO₃H⁻ site (i.e. HPO₄²⁻) ion before linked to the surface as a predominant species at closest physiological pH. In particular, it can be noted that the presence of the

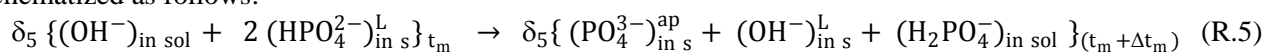
neutral site $\equiv\text{OPO}_3\text{H}_2$ (*i.e.* H_2PO_4^- ion before linked to the surface) is zero over a large pH interval ($3.5 < \text{pH} < 11$). Thus, the surface speciation of deficient apatite is free of $\equiv\text{H}_2\text{PO}_4$ at pH values around 7.4. While, in this pH region, the speciation diagram for the orthophosphate species in aqueous solution depicts that the negatively charged species H_2PO_4^- and HPO_4^{2-} prevail in the solution with equal quantities practically. Then, it is clear that H_2PO_4^- groups are unstable thermodynamically into interfacial hydrated shells of NHA's nanocrystals. Then, they are released into maturation solution. As a result, the following reaction equation illustrates the events associated with the HP^{L} decrease:



where, the subscript letters “in s” and “in sol” indicate “in the solid phase” and “in the ageing solution” respectively.

Thus the loss of HP^{L} entities, which induces the decrease of total phosphorus mole number (P), causes an increase of Ca/P atomic ratio with maturation time. In fact, simultaneously with this reaction, the change of $\frac{\text{Ca}}{\text{P}}$ ratio is inversely strongly correlated to HP^{L} ($r_{1,2}^{\text{t}} = -0.915$, $p < 0.01$). This association can be represented as follows: “ $n_{\text{Ca}^{2+}} = 10.26 (\pm 0.07) - 1.78 (\pm 0.64)n_{\text{HP}^{\text{L}}}$ ” ($\sim 6 \times [E_{1,2}^{\text{t}}]$), in order to lead Ca/P ratio to the Ca^{2+} mol. number per mol. of apatite). Thus, we find that during apatite maturation the improvement of one mole of calcium is strongly associated with the decrease of two moles of HP^{L} , one of them is released in the ageing solution as H_2PO_4^- species, in agreement with the scheme (R.4). As a result, an imbalance of negative charge occurs into the apatite. These evolutions clearly support the insertion of the most mobile anion from the ageing solution in nanocrystals despite the chemical reactivity in the hydrated layers such as the water dissociation. However, chemical formula (F.1) shows the increase of OH^- anions in the first period of maturation. The migration of OH^- will compensate the disappearance of H_2PO_4^- groups to equilibrate the charge balance of the two neighbouring environments: ageing solution and NHA's hydrated shells. This suggests that the changes of OH^- and HP^{L} will be correlated. In this context, it should be noted that the use of the correlation statistical test implies automatically no random variables [42]. As the number of OH^- mole has not been obtained experimentally (at random), but with conscious decision using a calculation based on the maintaining of the electric neutrality, it cannot be considered as random variable. So, we cannot use this variable in the correlation statistical test and conclusions are made only on correlations with the apatitic OH^- ions (OH^{ap}). At the earliest step (up to the release of the hydration water) no significant change of the OH^{ap} species is observed, also, it has no significant correlation with the water and PO^{L} groups as shown in Table 2. Thus, it seems that during the short early age (up to 1 day in our experimental conditions) of the nascent nanocrystals, the scattered OH^- ions are mainly localized in the hydrated layer. According to the chemical formula change without increase of the apatitic OH^- species up to 1 day, the increase of total OH^- ions confirms this point of view. Thus, at the first stage of the maturation process, the main event associated with the quick decrease of HP^{L} during the maturation, is the release of HPO_4^{2-} ions in the fluid environment.

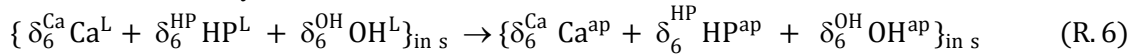
This phenomenon occurs with the increase of the Ca/P ratio, PO^{ap} and OH^{L} amount, without input of $n_{\text{Ca}^{2+}}$ into NHA's nanocrystals or output of water. So, if OH^- groups are the most mobile anions in a liquid environment, the scheme illustrating the main continuous event involving HP^{L} with the maturation time (t_{m}), can be schematized as follows:



where: the subscript letters “in s” and “in sol”, indicate “in the solid phase” and “in the ageing solution” respectively.

Our finding validates the previously proposed maturation process of Rey *et al.*, involving proton overlapping between two labile HPO_4^{2-} ions with the eventual rejection of H_2PO_4^- in solution [9,25]. Furthermore, with the dehydration beginning, HP^{L} change remains not significantly correlated to water amount as stated by the correlation matrix not shown here (NS). However, it becomes strong negative linear associated with OH^{ap} ($r_{1,4}^{\text{II}} = -0.983$, $p < 0.01$) and HP^{ap} ($r_{1,3}^{\text{II}} = -0.892$, $p < 0.05$) amount, this latter is strongly correlated to the Ca/P ratio (NS: $r_{\text{Ca/P,HP}^{\text{ap}}}^{\text{II}} = 0.822$, $p < 0.1$) and OH^{ap} (NS: $r_{\text{OH}^{\text{ap,HP}^{\text{ap}}}^{\text{II}}} = 0.925$, $p < 0.05$). These results indicate obviously the relocation of these ions to enable the stability through the creation of the cation-anions bound in the building of the prefiguring apatitic domains containing apatitic Ca^{2+} , HPO_4^{2-} and OH^- ions, as shown in our chemical formula. The presence of the prefiguring apatitic domains was predicted by Rodriguez and Lebugle to describe the gradual crystallization of the amorphous phosphate into deficient hydrated apatite [32]. Recently, it has been confirmed that the surface hydrated layer covering the NHA's crystalline core is amorphous, and so is

the hydrated shell surrounded mature bone mineral particles [13,15, 29, 48-50]. Added to that, with the release of water, PO^{ap} is partially explained by the PO^L decrease ($r_{2,1}^{II} = -0.834$, $p < 0.1$). The predominant relocations ($p < 0.05$) could be illustrated by this scheme:



Indeed, this scheme indicates that the water molecules are not involved in the ions rearrangement. So, how could the water release enhance these relocations? Here, we highlight that before significant loss of water, the OH⁻ ions incorporated into the apatite mainly concentrate on the hydrated layers as labile species (R.5), so the amount of OH^L will increase. The water release will induce the increase of the labile ion concentration in the hydrated shells, creating a concentration gradient along the interface between crystalline core edges and hydrated layers. In consequence, there's the diffusion (relocation) of labile entities from the hydrated shell into the incomplete unit cells surrounding the apatitic core, to favor the formation of the nanocrystals in aqueous media. Moreover, it has been pointed out, using several methods that the elimination with time of solvation water molecules is crucial to the junction of the apatitic prefiguring domains in order to develop the stable apatite domains [32,40,47,51].

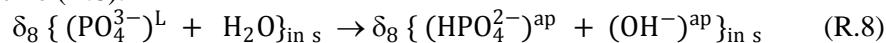
Considering the concentration gradient, it has been reported that the most likely mobile ions are Ca²⁺ and OH⁻ in the deficient apatite at lower temperature [52]. So, the OH⁻ and Ca²⁺ motions from the hydrated shells, which are relatively disordered compared to the apatitic domains to the interfacial local area prefiguring the apatitic domains under building, can be spontaneous. Indeed, it has been shown in previous work that the fraction of PO₄³⁻ ions, without specifying if it is labile or apatitic PO₄³⁻ species, can react with tightly bond water molecules to produce both HPO₄²⁻ and OH⁻ entities [53]. This reaction, which is currently named 'internal hydrolysis of apatite', is schematized by the following equation [54]:



Hence, the internal hydrolysis is particularized in relation to the other maturation events by consumption of water that is why this latter would be inversely correlated with both HPO₄²⁻ and OH⁻ apatitic species.

According to our statistical data, H₂O change, which has positive correlation with the slow decrease of PO^L groups ($r = 0.834$, $p < 0.1$) are inversely strongly associated with both HP^{ap} ($r_{3,3}^{II} = -0.966$, $p < 0.01$) and OH^{ap} change ($r_{3,4}^{II} = -0.823$, $p < 0.1$). Indeed, the linear relationships involving water molecules as reactant seem to have comparable minuscule slopes (Table 2: [E_{3,3}^{II}] and [E_{3,4}^{II}]). This apparent similarity proves that very weak fraction of the hydration water can interact with PO₄³⁻ groups due, to the presence of the few water molecules linked strongly to these ions, as identified by NMR spectroscopy [15,29,49,55,56].

An important question arises: among apatitic and labile PO₄³⁻ ions which are the predominant entities reacting with water molecules? Up to the water release, PO^L has no influence on both OH^{ap} and HP^{ap} changes (H₀ is not rejected). After significant decrease of water, it becomes strongly and inversely correlated to these apatitic species ($r_{2,4}^{II} = -0.934$ and $r_{2,3}^{II} = -0.891$, $p < 0.05$) in accordance to the internal hydrolysis reaction. Controversially, PO^{ap} change is never correlated significantly with HP^{ap}. These statistical results seem to support more the input of the labile PO₄³⁻ groups than the apatitic ones. Thus, the internal hydrolysis can be presented with the noted scheme (R.8).



In order to confirm that (HPO₄³⁻)^{ap} and OH⁻ entities evolve in both relocation of labile species (R.6) and internal hydrolysis (R.8), bivariate linear regressions between all involving apparently independent variables (having an insignificant multicollinearity: VIF < 3 [57]) are tested and calculated. Some validated bivariate equations are grouped in Table 4. It shows that both the increases of the two apatitic (HPO₄²⁻)^{ap} and (PO₄³⁻)^{ap} groups [E_{Biv}(I)] are strongly associated with the alteration of (HPO₄²⁻)^L groups in agreement with both their relocation (R.6) and the deprotonation event (R.4) respectively. Moreover, the progressive increase of both (HPO₄²⁻)^{ap} and (OH⁻)^{ap} amount can be explained by the decrease of (HPO₄²⁻)^L groups in respect with the relocation process (R.6) and the reduction of very little water fraction.

In addition, the OH^{ap} formation is also possible through HPO₄²⁻ hydrolysis as follow:



This proposal implies that the OH^{ap} formation consumes more water quantity than that consumed in HP^{ap} formation through the PO^L internal hydrolysis (R.8), in opposite of our findings.

According to the bivariate regressions $[E_{\text{Biv}}(\text{II})]$ and $[E_{\text{Biv}}(\text{III})]$, the same water amount is consumed (the same coefficient value in the regressions: 0.01) to regenerate $(\text{HPO}_4^{2-})^{\text{ap}}$ and $(\text{OH}^-)^{\text{ap}}$ entities respectively. This is in agreement with stoichiometric ratio of the internal hydrolysis reaction (R.8): $\frac{v_{(\text{OH}^-)^{\text{ap}}}}{v_{(\text{HPO}_4^{2-})^{\text{ap}}}}: \frac{1}{1}$. Therefore, we deduce

that the HPO_4^{2-} hydrolysis is not significant and the main route of the apatite hydroxylation is the PO_4^{L} internal hydrolysis (R.8).

With maturation time, the dissolution enthalpy becomes more negative indicating more stability of the NHA's nanocrystals [34]. This is in perfect agreement with other authors who showed that the decrease of NHA's labile environments induces an increase of their stability which leads to a decrease of their reactivity with age [9,25,30]. This result shows the establishment of the more energetic bonds inside nascent apatitic domains which are progressively formed as pointed out by the increase of the maturity index [58].

According to the data in Table 3, the dissolution enthalpy is rather strongly associated to the decrease of HP^{L} groups (see $[E_{1,6}^{\text{I}}]$) and to the water release (see $[E_{3,6}^{\text{II}}]$) in the first and the second periods respectively. It is clear that the thermodynamic results corroborate with the existence of two phases in the maturation process.

Table 4: Correlations coefficients and significant bivariate linear equations correlate: first the $(\text{HPO}_4^{2-})^{\text{L}}$ species changes with apatitic phosphate ones ($[E_{\text{Biv}}(\text{I})]$) and second each internal hydrolysis product $(\text{HPO}_4^{2-})^{\text{ap}}$ change ($[E_{\text{Biv}}(\text{II})]$) or $(\text{OH}^-)^{\text{ap}}$ one ($[E_{\text{Biv}}(\text{III})]$) with the alterations of $(\text{HPO}_4^{2-})^{\text{L}}$ and H_2O entities, with NHA's ageing.

Explained variable (Y_i)	Explaining variables ($X_{k,i}$)	VIF	Equation
$(\text{HPO}_4^{2-})^{\text{L}}$	$(\text{PO}_4^{3-})^{\text{ap}}$ and $(\text{HPO}_4^{2-})^{\text{ap}}$	1.89	$[E_{\text{Biv}}(\text{I})]$ $(\text{HPO}_4^{2-})^{\text{L}} = 0.67 - 0.72 (\text{HPO}_4^{2-})^{\text{ap}} - 0.71 (\text{PO}_4^{3-})^{\text{ap}}$, $p < 0.05$ $r = 0.989$, $R^2 = 0.979$.
$(\text{HPO}_4^{2-})^{\text{ap}}$	$(\text{HPO}_4^{2-})^{\text{L}}$ and $n_{\text{H}_2\text{O}}$	2.31	$[E_{\text{Biv}}(\text{II})]$ $(\text{HPO}_4^{2-})^{\text{ap}} = 0.17 - 0.01 n_{\text{H}_2\text{O}} - 0.26 (\text{HPO}_4^{2-})^{\text{L}}$, $p < 0.05$ $r = 0.997$, $R^2 = 0.995$.
$(\text{OH}^-)^{\text{ap}}$			$[E_{\text{Biv}}(\text{III})]$ $(\text{OH}^-)^{\text{ap}} = 0.26 - 0.01 n_{\text{H}_2\text{O}} - 0.54 (\text{HPO}_4^{2-})^{\text{L}}$, $p < 0.1$ $r = 0.991$, $R^2 = 0.982$.

✓ Why aren't the OH^- ions detected in NHA's nascent nanocrystals as in young bone mineral?

Concerning the microstructural (L_c , L_a) and micro textural (I_{cr} , ϵ) parameters change, our findings show that at the earliest period, no significant correlation between these features and labile groups is validated. Simultaneously to the output of the water and the increase of the apatitic OH^- content, the nanocrystals' microstructural parameters (I_{cr} , L_c and L_a) become inversely correlated to the hydrated layer species, whereas, the micro-strain coefficient (ϵ) has a strong positive association with HP^{L} . These correlations support the decrease of the disorder and the dislocation at the expense of the labile species and the increase of apatitic ones with the occurring maturation processes. In fact, OH^{ap} is positively strongly correlated to lattice parameters L_c ($r_{\text{OH}^{\text{ap}},L_c}^{\text{II}} = 0.951$, $p < 0.05$) and L_a ($r_{\text{OH}^{\text{ap}},L_a}^{\text{II}} = 0.909$, $p < 0.05$). Thus, the increase of OH^{ap} ions is involved in the expansion of the crystal. Moreover, OH^{ap} has strong and positive correlation with crystallinity index ($r_{\text{OH}^{\text{ap}},I_{\text{cr}}}^{\text{II}} = 0.938$, $p < 0.05$). Thus, our findings prove that the main requirement for the apatitic OH^- formation is the improvement of the NHA's nanocrystals structural order (*i.e.* network defects and strain decreases), which is caused by an increase of apatitic species through the alteration of the hydrated layer entities leading to the enlargement of crystals parameters. These results are consistent with previous works findings based on the microstructural properties [7- 9,29]. In fact, among the several events occurring

with maturation only the internal hydrolysis imply, independently of the chemical composition of the ageing fluid, the formation of the apatitic OH^- species which promote the formation of the NHA's aggregate cells building the hydroxylated apatite network. This process requires adequate preparation of the prefiguring units through the relocation of some labile entities as well as the labile HPO_4^{2-} deprotonation into apatitic PO_4^{3-} ions, which occurs simultaneously with the incorporation of the most mobile anions from the surrounding liquid fluid (ageing or physiological liquid environments). If the latter is free of foreign anions, these ions are the hydroxyl ones at body's pH or certainly basic one. Nonetheless, if the surrounding liquid contains more mobile monovalent or bivalent anions, as F^- or CO_3^{2-} in the body's fluid, the most mobile ones migrate to the hydrated shells, and diffuse to stabilize the prefigured cells (the prenucleation clusters, as namely by Dorvee and Veis [49,50]) into nascent nanocrystals free of hydroxyl ions as shown in the immature bioapatites crystals. Thus, this

phenomenon explains why the OH⁻ ions are not detected in the young bone mineral. In the ageing ones, the improvement of the hydroxyl ions is due to their production through the internal hydrolysis process of the rather labile PO₄³⁻ groups likely trapped with the closest water molecules inside the prenucleation clusters building the hydroxylated deficient-apatite nanocrystals.

Conclusions

Using univariate and bivariate linear statistical treatments, we have established the correlation between the changes of all NHA physicochemical features with maturation time. The obtained data confirm that the maturation process is realized through three events, two of which are strongly related to the water removal. The first event is predominant at the earliest ageing period despite the water release. It is a continuous process involving the deprotonation of the labile HPO₄²⁻ species into apatitic PO₄³⁻ ones. This phenomenon needs the migration of most mobile anions from the surrounding fluid, as F⁻ or CO₃²⁻ ions and also OH⁻ ones, into nanocrystals hydrated shells. The two other simultaneous events become significant with the water reduction (release and consumption). First, the relocation of the labile species will prefigure the aggregates (clusters) building the nanocrystals to favor the stability of the most mobile anions on c-axis channel sites. Second, there is the production of the apatitic OH⁻ ions through the PO₄³⁻ hydrolysis. We highlighted for the first time that the main cause of the aged NHA hydroxylation is the internal hydrolysis of labile PO₄³⁻ groups and not apatitic ones. Such reaction takes place only if some order is established to permit the trapping of neighboring H₂O and PO^L to promote the contacting of these reagents. Kinetically, the maturation process follows two phases in respect to the change of the hydrated shell entities. The first rapid phase occurs with the crucial decrease of the labile HPO₄²⁻ ions whereas the second takes place with both water and labile PO₄³⁻ species decrease.

From a thermodynamic point of view, the NHA's reactivity is rather dependent on the deprotonation process involving labile HPO₄²⁻ in the nascent nanocrystals whereas it's monitored by the events involving water molecules (the relocation and the internal hydrolysis) in the aged crystals. Nevertheless, the labile entities and water molecules bonds are less energetic, so, they can't be the direct cause of the measured enthalpy evolution. Then, this variation may be the result of other phenomena that should be investigated. These findings elucidated that the controversies concerning the NHA's ageing are apparent. In fact, all the hydrated shell entities (HP^L, PO^L and H₂O) are involved in NHA maturation process and they are correlated to the other physicochemical NHA's crystals features. Moreover, the correlation between the lack of OH⁻ ions, the increasing structural disorder and the decreasing crystal size is due to the fact that the hydroxyl ions formation is related to water release and consumption. This loss of water will enhance the labile species relocation and labile phosphate internal hydrolysis, which will ameliorate the structural lattice organization and reduce the micro distortions. We conclude that the high ability of the hydrated layer species to alter into apatitic ones is at the origin of the more stable but less reactive apatitic domains, which are the driving force behind in the NHA's maturation process. Their evolutions, according to various maturation phenomena, will cause changes in apatite structural and textural features.

Besides, our data suggest that the bone-mineral remodeling is realized through the three described events of the maturation process. Then, the presence of the apatitic OH⁻ in the bone mineral could be considered as the marker of its ageing as well as its less reactivity. Hence, the detection of apatitic OH⁻, the water decrease or /and labile PO₄³⁻ alteration, can be used as an indicator of precocious bone senescence. This comprehensive study leads, in particular, to a better understanding of how each hydrated shell entity affects the physicochemical properties characteristics of NHA's crystals and their reactivity. Consequently, this will eventually lead to control the process for producing biomaterials with desirable bioactivity through the control of the hydrated shell entities alteration.

Acknowledgments-The authors thank F. Mokhtar (CNRSM) and A. Bel Haj Amara (FSB) for the reagent provision and experimental supports.

References

1. Boskey A.L., Coleman R. *J. Dent. Res.* 89 (2010) 1333.
2. Elliott J.C., Wilson R.M., Dowker S.E.P. *JCPDS-International Centre for Diffraction Data Advances in X-ray Analysis.* 45 (2002) 172.
3. Weiner S., Wagner H.D. *Annu. Rev. Mater. Sci.* 28 (1998) 271.
4. Silva R.F., Da Silva Sasso G.R., Cerri E.S., Simoes M.J., Cerri, P.S. *BioMed Res. Int.* 2015 (2015) 1.

5. Vallet-Regi M. *Dalton Trans.* 28 (2006) 5211.
6. Rey C., Miquel J.L., Facchini L., Legrand A.P., Glimcher M.J. *J. Bone* 16 (1995) 583.
7. Wopenka B., Pasteris J.D. *Mater. Sci. Eng. C* 25 (2005) 130.
8. Pasteris J.D., Wopenka B., Freeman J.J., Rogers K., Jones E.V., Van Der Houwen J.A.M., Silva M.J. *Biomaterials* 25 (2004) 229.
9. Rey C., Combes C., Drouet C., Cazalbou S., Grossin D., Brouillet F., Sarda S. *Prog. Cryst. Growth Charact. Mater.* 60 (2014) 63.
10. Kaflak A., Kolodziejski W. *Magn. Reson. Chem.* 46 (2008) 335.
11. Bertinetti L., Tampieri A., Landi E., Ducati C., Midgley P.A., Coluccia S., Martra G. *J. Phys. Chem. C* 111 (2007) 4027.
12. Wilson E.E., Awonusi A., D Morris M., Kohn D.H., Tecklenburg M.M.J., Beck L.W. *J. Bone Miner. Res.* 20(4) (2005) 625.
13. Sakhno Y., Bertinetti L., Iafisco M., Tampieri A. Roveri N., Martra G. *J. Phys. Chem. C* 114(2010) 16640.
14. Eichert D., Sfihi H., Combes C., Rey C. *Key Eng. Mater.* 254-256 (2004) 927.
15. Pajchel L., Kowalska V., Smolen D., Kedzierska A., Pietrzykowska E., Lojkowski W., Kolodziejski W. *Mat. Res. Bull.* 48 (2013) 4818.
16. Bracci B., Torricelli P., Panzavolta S., Boanini E., Giardino R., Bigi A. *J. Inorg. Biochem.* 103 (2009) 1666.
17. Eichert D., Combes C., Drouet C., Rey C. *Key Eng. Mater.* 3 (2005) 284.
18. Bertinetti L., Drouet C., Combes C., Rey C., Tampieri A., Coluccia S., Martra G. *Langmuir* 25 (10) (2009) 5647.
19. Cazalbou S., Eichert D., Ranz X., Drouet C., Combes C., Harmand M.F., Rey C. *J. Mater. Sci. Mater. Med.* 16 (2005) 405.
20. El Rhilassi A., Mourabet M., El Boujaady H., Ramdane H., Bennani-Ziatni M., El Hamri R., Taitai A., *J. Mater. Environ. Sci.* 3 (3) (2012) 515.
21. Eanes E.D., Meyer J.L. *Calcif. Tiss. Res.* 23 (1977) 259.
22. El Rhilassi A., Mourabet M., El Boujaady H., Bennani-Ziatni M., El Hamri R., Taitai A. *J. Mater. Environ. Sci* 5 (5) (2014) 1442.
23. Cazalbou S., Combes C., Eichert D., Rey C., Glimcher M.J. *J Bone Miner. Metab.* 22 (2004) 310.
24. Bensaoud A., Bouhaous A., Ferhat M. *Z. Naturforsch.* 55 a (2000) 883.
25. Rollin-Martinet S., Navrotsky A., Champion E., Grossin D., Drouet C. *J. Am. Mineralogist.* 98 (2013) 2037.
26. Loong C.K., Rey C., Kuhn L.T., Combes C., Wu Y., Chen S.H., Glimcher M.J. *Bone* 26(6) (2000) 599.
27. Glimcher M.J. The nature of the mineral phase in bone: biological and clinical implications. In: Avioli LV, Krane SM, ed., *Metabolic bone disease and clinically related disorders*. Academic Press, (1998) 23.
28. Cho G., Wu Y., Ackerman J.L. *Science* 300 (5622) (2003) 1123.
29. Pajchel L., Kolodziejski W. *J. Nanopart Res.* (2013) 1868.
30. Hina A., Réactivité du minéral osseux et des analogues de synthèse, Thèse, INP Toulouse, (1997).
31. Charlot G., *Les Méthodes de la Chimie Analytique*, Masson, (1966).
32. Rodrigues A., Lebugle A. *Colloids Surfaces A: Physicochem. Eng. Aspects.* 145 (1998) 191.
33. Kibalczyk W., Christoffersen J., Christoffersen M.R. Zielenkiewicz A., Zielenkiewicz, W. *J. Crystal Growth.* 106 (1990) 355.
34. Somrani S., Banu M., Jemal M., Rey C. *J. Solid State Chem.* 178 (2005) 1337.
35. Mittemeijer E.J., Welzel U., *Z. Kristallogr.* 223 (2008) 552.
36. Landi E., Tampieri A., Celotti G., Sprio S. *J. European Ceramic Soc.* 20 (2000) 2377.
37. Delhez R., De Keijser Th. H., Mittemeijer E.J., *Fresenius Z. Anal Chem.* 312 (1982) 1.
38. M. Banu, Mise en forme d'apatites nanocristallines: Ceramiques et ciments, Thèse, INP Toulouse, (2005).
39. Miller L.M., Vairavamurthy V., Chance M.R.; Mendelsohn, R., Paschalis E.P., Betts F., Boskey A.L. *Biochimica et Biophysica Acta.* 1527 (2001) 11.

40. Apfelbaum F., Mayer I., Rey C., Lebugle A. *J. Cryst. Growth*. 144 (1994) 304.
41. De Bourmont, M. *Comptabilités et Innovation* (2012). <https://hal.archives-ouvertes.fr/hal-00691156>.
42. MC Donald J.H. *Handbook of Biological Statistics*, Sparky House, (2008).
43. Bewick V., Cheek L., Ball J. *Critical Care*. 7 (2003) 451.
44. Rumsey D., *Statistics Essentials for Dummies*, Wiley, (2010).
45. De Winter J.C.F. *Practical Assessment, Research & Evaluation*, 18 (10) (2013) 1.
46. Joseph J.F. Hair., Black Barry C. W., Babin. J. *Multivariate Data Analysis*, Prentice Hall (2009).
47. Bengtsson A., Shchukarev A., Persson P., Sjoberg S. *Geochim. Cosmochim. Acta*. 73 (2009) 257.
48. Wang Y., Euw S.V., Fernandes F.M., Cassaignon S., Selmane M., Laurent G., Pehau-Arnaudet G., Coelho C., Bonhomme-Coury L., Giraud-Guille M.M., Babonneau F., Azaïs T. Nassif, N. *Nature Mat.* (2013) 1.
49. Dorvee J.R., Veis A. *J. Structural Biology*. 183 (2013) 278.
50. Veis A., Dorvee J. R. *Calcif. Tissue Int.* (2012) 1.
51. Somrani S., Rey C., Jemal M. *J. Mater. Chem.* 13 (2003) 888.
52. Royce B. *J. Phys. Colloq.* 34 (1973) C9-327.
53. Rey C., Combes C., Drouet C., Glimcher M.J. *Osteoporos Int.* 20 (6) (2009) 1013.
54. Heughebaert J.C. Contribution à l'étude de l'évolution des orthophosphates de calcium précipités amorphes en orthophosphates apatitiques, thèse, INP Toulouse (1977).
55. Wilson E.E., Awonusi A., Morris M.D., Kohn D.H., Tecklenburg M.M.J., Beck L.W. *Biophysical J.* 90 (2006) 3722.
56. Jager C., Welzel T., Meyer-Zaika W., Epple M. *Magn. Reson. Chem.* 44 (2006) 573.
57. O'Brien R. M. *Quality & Quantity* 41 (2007) 673.
58. Farlay D., Panczer G., Rey C., Delmas P., Boivin, G. *J. Bone Miner. Metab.* 28 (2010) 433.

(2016) ; <http://www.jmaterenvironsci.com/>

Appendix: Steps of Statistical calculation

1. Correlation coefficient determination

For linear correlation, the correlation coefficient $r_{X_{k,i}, Y_i}$ is essentially a measure of linear association between two paired variables $X_{k,i}$ and Y_i . It is given by the Person's relation:

$$r_{X_{k,i}, Y_i} = \frac{\sum_{i=1}^n (X_{k,i} - \bar{X})(Y_i - \bar{Y})}{\sqrt{\sum_{i=1}^n (X_{k,i} - \bar{X})^2 \sum_{i=1}^n (Y_i - \bar{Y})^2}} \quad [\text{E.1}], \text{ where } \bar{X} \text{ and } \bar{Y} \text{ are the means from } X_{k,i} \text{ and } Y_i \text{ values respectively}$$

[43]. This statistic coefficient measures the strength and direction of a linear relationship between the pairs variables $\{X_{k,i}, Y_i\}$ on a scatter plot. It is negative (or positive) when two paired variables $X_{k,i}$ and Y_i are in an inverse (or similar) behavior. According to Rumsey, there is a perfect linear relationship, if $|r_{X_{k,i}, Y_i}|$ exactly equals to 1. If there is strong, moderate or weak linear association, the result will be 0.70, 0.50 or 0.30 respectively. Then, if this coefficient is null, no linear relationship is given. Therefore, to prevent any over-interpretation of the degree to which two variables are correlated (due to the small population size here), we will focus only on the strong associations. Thus, we test the significance of the correlation coefficient if $|r_{X_{k,i}, Y_i}| > 0.8$ [44].

2. Correlation significance

Statistical significance is a purely probabilistic statement regarding the chance of observing a particular result. To be confident that the studied variables are related t-test have to be performed. For typical samples the significance of a correlation value must be tested using the Fisher t-distribution. If the sample size, n , is not large ($n < 20$), the estimated value of the population standard deviation is itself subject to uncertainty. So the

confidence intervals need to be larger still. In this case, a small-sample approximation to the Normal is used, known as the Fisher t-distribution [42,45]. In the case of the t-distribution approach, the following expression is calculated and then compared with critical values of the t-distribution table on n-2 degrees of freedom:

$$t_{r_i} = r_{X_{k,i}, Y_i} \sqrt{\frac{n-2}{1-r_{X_{k,i}, Y_i}^2}} \quad [E.2]$$

Moreover, if t_{r_i} is superior to $t_{0.01, n-2}$, $t_{0.05, n-2}$ or $t_{0.1, n-2}$, $r_{X_{k,i}, Y_i}$ is significant at 99% (or $p < 0.01$, with p is the probability of the obtaining observed effect under a null hypothesis (H_0)), 95% (or $p < 0.1$) and 90% (or $p < 0.1$) respectively. Then, we are going to determine the linear regression.

3. Estimation of the regression

3.1 Calculation of the OLSM's estimators:

The least squares estimators are given in equations [E.3] and [E.4] for the slop ($\beta_{1,i}$) and intercept ($\beta_{0,i}$) respectively [45]:

$$\widehat{\beta}_{1,i} = \frac{\sum_{i=1}^n (X_i - \bar{X})(Y_i - \bar{Y})}{\sum_{i=1}^n (X_i - \bar{X})^2} \quad [E.3] \quad \text{and} \quad \widehat{\beta}_{0,i} = \bar{Y} - \widehat{\beta}_{1,i} \bar{X} \quad [E.4]$$

3.2 Test of the OLSM's mathematical model

Besides, to make sure that Y_i and $X_{k,i}$ are related and the estimators are significant, we use significance test of $\widehat{\beta}_{1,i}$ and $\widehat{\beta}_{0,i}$ where $t_{1,i}$ and $t_{0,i}$ have to be calculated as follows:

$$t_{1,i} = \frac{\widehat{\beta}_{1,i}}{s(\widehat{\beta}_{1,i})} \quad [E.5] \quad \text{and} \quad t_{0,i} = \frac{\widehat{\beta}_{0,i}}{s(\widehat{\beta}_{0,i})} \quad [E.6]$$

Where $s(\widehat{\beta}_{1,i})$ and $s(\widehat{\beta}_{0,i})$ are the standard errors of the slop ($\beta_{1,i}$) and intercept ($\beta_{0,i}$) respectively. They are calculated, using the standard error of the estimate: $s = \sqrt{\frac{\sum_{i=1}^n (Y_i - \hat{y}_i)^2}{n-2}}$ where, \hat{y}_i is the estimated value using the regression, according to the following equations:

$$s(\widehat{\beta}_{1,i}) = \frac{s}{\sqrt{\sum_{i=1}^n (X_i - \bar{X})^2}} \quad [E.7] \quad \text{and} \quad s(\widehat{\beta}_{0,i}) = s \sqrt{\frac{1}{n} + \frac{\bar{X}^2}{\sum_{i=1}^n (X_i - \bar{X})^2}} \quad [E.8]$$

So, when both $t_{1,i}$ and $t_{0,i}$ are superior to $t_{0.01, n-2}$, $t_{0.05, n-2}$ or $t_{0.1, n-2}$, $\beta_{1,i}$ and $\beta_{0,i}$ are significant at 99%, 95% or 90% respectively. Then, we can conclude that control variable may have a chance to affect the outcome (explained variable) and that the null hypothesis is rejected [46].

(2016) ; <http://www.jmaterenvirosnci.com/>